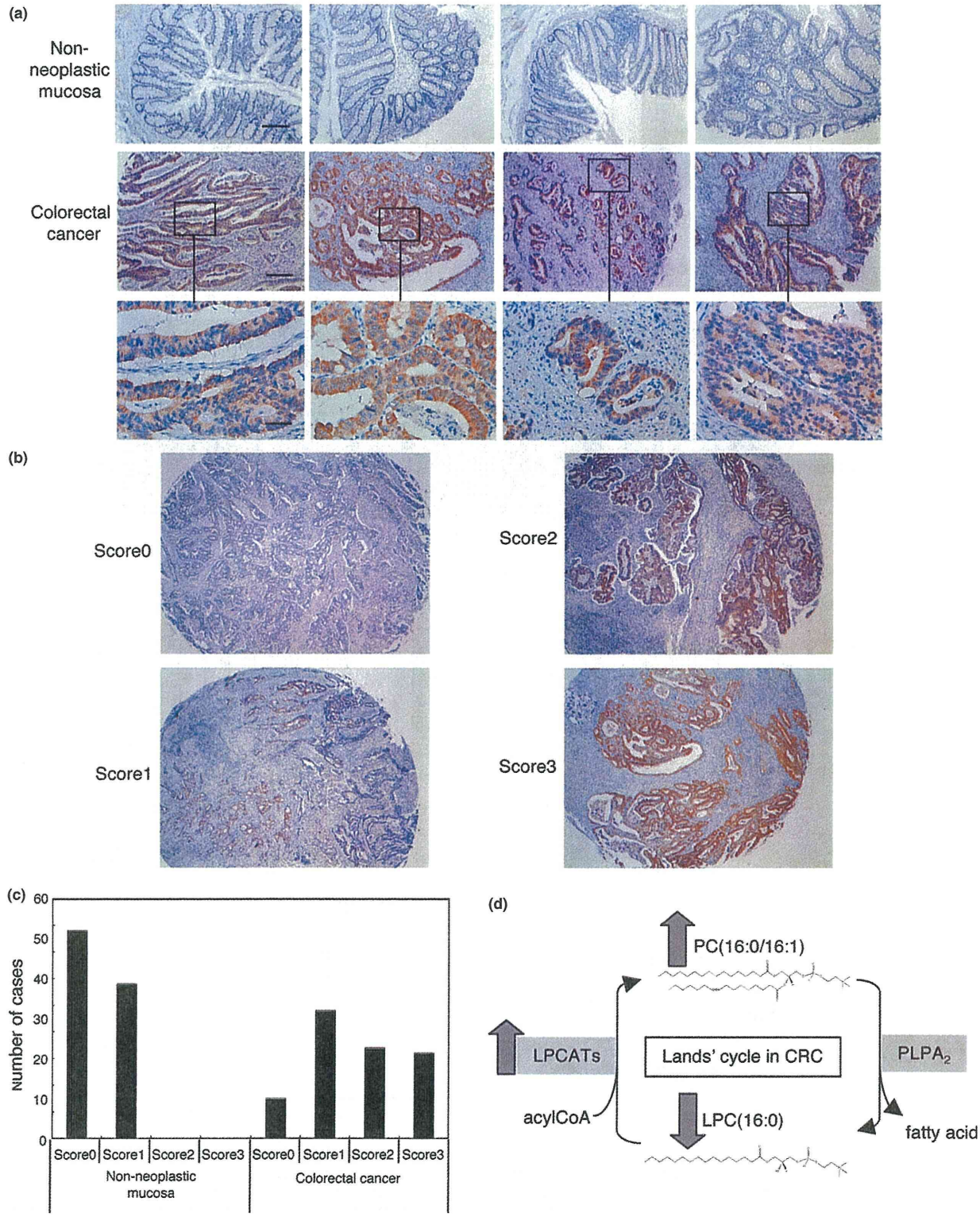

Fig. 4. Immunohistochemical analysis of the expression of LPCAT4 in a tissue microarray (TMA). (a) Non-neoplastic mucosa (top) and corresponding colorectal cancer (CRC) (middle) were stained for LPCAT4 expression using anti-LACAT4 antibody. Higher magnification images from CRC are also shown (bottom). Top, middle, ×10; bottom, ×40. Bar, 200 μm (top, middle) and 10 μm (bottom). (b) Representative scoring images. (c) Levels of LPCAT4 expression evaluated according to the scoring system described in the Materials and Methods section. The expression scores for all cases (272 cases) were examined and are presented in the graph. (d) Model of Land's cycle in CRC. LPCAT activities are elevated in CRC, which results in the increase of PC(16:0/16:1). LPCAT, lyso-PC acyltransferase.

doi: 10.1111/cas.12221

HCT116 cells were transfected with siRNA targeting LPCAT1, LPCAT2, LPCAT3 and LPCAT4. The knockdown efficiencies were evaluated using qPCR (Fig. 3b). The same experiments were also performed using DLD1 cells (Fig. S1A). The level of PC(16:0/16:1) was significantly decreased by the transfection of LPCAT4 siRNA (Fig. 3d). In DLD1 cells, the reduction of PC(16:0/16:1) was also observed in two of three LPCAT4 siRNA (Fig. S1B). The decrease in PC(16:0/16:1) was visually confirmed using the mass microscope (Fig. 3c). The LPCAT activities were analyzed using a LPCAT assay (Fig. 3e). The ratios of PC(16:0/16:1)/lyso-PC(16:0) were decreased in two of three siRNA targeted for LPCAT4. In two LPCAT1 siRNA, the ratios were also reduced. To investigate the effect of LPCAT4 expression on the growth of colon cancer cells, the cell growth was analyzed when transfected with LPCAT4 siRNA. The expression of LPCAT4 protein was significantly decreased (Fig. 3f). The knockdown of LPCAT4 caused delayed growth (Figs 3g, S1C). In Figure S1(C), cell growth was not inhibited by the transfection of siRNA targeted for LPCAT1 (siLPCAT1#1), which is likely because of the off-target effect of siRNA. To further confirm the involvement of LPCAT4 in CRC progression, we examined the expression of LPCAT4 immunohistochemically. A total of 272 tissue samples (136 benign and 136 CRC; Table S1) were stained for LPCAT4 expression and a total of 100 adenomas (Table S2) were also analyzed. LPCAT4 immunoreactivity was stronger in CRC than in the non-tumor mucosa and its expression seems to be in the endoplasmic reticulum in the cytoplasm (Fig. 4a). Stromal cells were not stained with LPCAT4 antibody. The stainings with four defined categories are shown in Figure 4(b). When immunohistochemical scores greater than 2 were considered, LPCAT4 was upregulated in 69% of the CRC samples (Fig. 4c). In contrast, the non-neoplastic mucosa displayed little or no LPCAT4 expression. Adenomas also had little staining with the LPCAT4 antibody (Fig. S2). The correlation between PC(16:0/16:1) expression measured using the mass microscope and the immunohistochemical score is shown in Table S3.

Discussion

In the present study, direct-tissue profiling using imaging MS was used to analyze the phospholipid patterns within human CRC and non-neoplastic colorectal mucosa. One of the unique starting points of the present study was the use of primary human cancer tissues, which are often difficult to handle, in the search for cancer biomarkers that have escaped previous investigators' attempts at identification. A PCA of the total mass spectra revealed separate clusters for CRC and the non-neoplastic mucosa (Fig. 1). According to the PCA and the corresponding loading plots, the *m/z* values that contributed to the separation of each group could be identified (Table 2). We also showed that the *m/z* value from the phospholipid PC(16:0/16:1) was differentially expressed in CRC and the non-neoplastic mucosa.

In the present study, a phospholipid analysis of CRC samples using imaging MS showed differences between CRC and the non-neoplastic mucosa (Fig. 2). PC(16:0/16:1) was specifically localized in CRC areas, demonstrating that PC(16:0/16:1) is a CRC marker. Thus, PC(16:0/16:1) is a novel CRC-specific biomarker. The simultaneous characterization of molecular information and histological structures using imaging MS is very useful in various clinicopathological settings, as previously reported by our group.[35–37] Currently, the mass microscope is the most powerful modality for identifying lipids. Consequently, imaging MS has the ability to overcome some of the weaknesses of immunohistochemistry. Direct analysis of the metabolome in cancer tissues could provide a more precise representation in tissues than that provided using other methods currently used in the field of pathology.

To investigate LPCAT activity in the present study, we examined the PC(16:0/16:1) and lyso-PC(16:0) cell membrane constituents. The ratio of PC(16:0/16:1)/lyso-PC(16:0) in CRC was higher than that in the non-neoplastic mucosa (Fig. 3a). The ratio was reduced when HCT116 cells were transfected with siRNA targeted for LPCAT1 and LPCAT4 (Fig. 3e). Therefore, this result supports the catalytic activation of LPCAT in CRC cells. Notably, the silencing of LPCAT4 reduced the PC(16:0/16:1) level and cell growth in the colon cancer cell line HCT116 and DLD1 *in vitro* (Figs 3d, S1B). Moreover, LPCAT4 was overexpressed in CRC (Fig. 4). LPCAT4 (also named MBOAT2) is one of the four mammalian LPCAT that have been cloned[33] and plays a catalytic role with a preference for fatty acid (FA)(16:1) and FA(18:1) in PC synthesis.[33,34] This finding suggests that enhanced reacylation of lyso-PC by LPCAT alters the amount of PC(16:0/16:1) in cancer cell membranes. The different influences of these four classes of the LPCAT family on human cancer cell characteristics have only been elucidated recently. The upregulation of LPCAT1 stimulated cell growth in the colon cancer cell line SW480.[8] Meanwhile, the knockdown of LPCAT3 by siRNA induced apoptosis and morphological changes in HEK293 cells.[38] Thus, LPCAT are involved in several aspects of tumorigenesis. Figure 4(d) is a model of PC(16:0/16:1) synthesys in CRC. In CRC, LPCAT activity is thought to be elevated, which results in increased production of PC(16:0/16:1).

We demonstrated that imaging MS can distinguish CRC from non-neoplastic mucosa based on their biomolecular signatures and can be used to identify phospholipid biomarkers. We showed that LPCAT4 contributes to PC(16:0/16:1) accumulation in CRC via the enhanced reacylation of lyso-PC. Further studies are necessary to conclude whether LPCAT4 is the sole factor responsible for the increase of PC(16:0/16:1) in CRC.

Acknowledgments

The authors are grateful to Hisaki Igarashi at the Department of Tumor Pathology, Hamamatsu University School of Medicine, for his excellent technical assistance in the cryostat sectioning. This work was supported by Grants-in-Aid (Research on International Cooperation in Medical Science, Grants-in-Aid for Cancer Research, 21-1) from the Ministry of Health, Labour and Welfare, the Japan Society for the Promotion of Science (22590356, 22790378, 23116510 and 20670004), the Ministry of Education, Culture, Sports, Science and Technology (221S0001), the Princess Takamatsu Cancer Research Foundation and the Smoking Research Foundation of Japan.

Disclosure Statement

The authors have no conflict of interest.

References

1 Boyle P, Levin B. *World Cancer Report 2008*. Lyon Cedex, France: WHO Press, 2008.

2 Dueck DA, Chan M, Tran K *et al.* The modulation of choline phosphoglyceride metabolism in human colon cancer. *Mol Cell Biochem* 1996; **162**: 97–103.

3 Dobrzynska I, Szachowicz-Petelska B, Sulkowski S, Figaszewski Z. Changes in electric charge and phospholipids composition in human colorectal cancer cells. *Mol Cell Biochem* 2005; **276**: 113–9.

4 Preetha A, Banerjee R, Huilgol N. Surface activity, lipid profiles and their implications in cervical cancer. *J Cancer Res Ther* 2005; **1**: 180–6.

5 White DA. The phospholipids composition of mammalian tissues. In: Ansell GB, Hawthorne JN, Dawson RMC, eds. *Form and Function of Phospholipids*. Amsterdam: Elsevier, 1973; 441–82.
6 Bishop WR, Bell RM. Assembly of phospholipids into cellular membranes: biosynthesis, transmembrane movement and intracellular translocation. *Annu Rev Cell Biol* 1988; **4**: 579–610.
7 Shindou H, Hishikawa D, Harayama T, Yuki K, Shimizu T. Recent progress on acyl CoA: lysophospholipid acyltransferase research. *J Lipid Res* 2009; **50**(Suppl.): S46–51.
8 Mansilla F, da Costa KA, Wang S *et al.* Lysophosphatidylcholine acyltransferase 1 (LPCAT1) overexpression in human colorectal cancer. *J Mol Med (Berl)* 2009; **87**: 85–97.
9 Woods AS, Jackson SN. Brain tissue lipidomics: direct probing using matrix-assisted laser desorption/ionization mass spectrometry. *AAPS J* 2006; **8**: E391–5.
10 McDonnell LA, Heeren RM. Imaging mass spectrometry. *Mass Spectrom Rev* 2007; **26**: 606–43.
11 Chaurand P, Sanders ME, Jensen RA, Caprioli RM. Proteomics in diagnostic pathology: profiling and imaging proteins directly in tissue sections. *Am J Pathol* 2004; **165**: 1057–68.
12 Cornett DS, Reyzer ML, Chaurand P, Caprioli RM. MALDI imaging mass spectrometry: molecular snapshots of biochemical systems. *Nat Methods* 2007; **4**: 828–33.
13 Seeley EH, Caprioli RM. Molecular imaging of proteins in tissues by mass spectrometry. *Proc Natl Acad Sci U S A* 2008; **105**: 18126–31.
14 Cazares LH, Troyer D, Mendrinos S *et al.* Imaging mass spectrometry of a specific fragment of mitogen-activated protein kinase/extracellular signal-regulated kinase kinase kinase 2 discriminates cancer from uninvolved prostate tissue. *Clin Cancer Res* 2009; **15**: 5541–51.
15 Morita Y, Ikegami K, Goto-Inoue N *et al.* Imaging mass spectrometry of gastric carcinoma in formalin-fixed paraffin-embedded tissue microarray. *Cancer Sci* 2010; **101**: 267–73.
16 Liu Y, Chen Y, Momin A *et al.* Elevation of sulfatides in ovarian cancer: an integrated transcriptomic and lipidomic analysis including tissue-imaging mass spectrometry. *Mol Cancer* 2010; **9**: 186.
17 Harada T, Yuba-Kubo A, Sugiura Y *et al.* Visualization of volatile substances in different organelles with an atmospheric-pressure mass microscope. *Anal Chem* 2009; **81**: 9153–7.
18 Kurabe N, Hayasaka T, Igarashi H *et al.* Visualization of phosphatidylcholine (16:0/16:0) in type II alveolar epithelial cells in the human lung using imaging mass spectrometry. *Pathol Int* 2013; **63**: 195–200.
19 Shimma S, Sugiura Y, Hayasaka T, Zaima N, Matsumoto M, Setou M. Mass imaging and identification of biomolecules with MALDI-QIT-TOF-based system. *Anal Chem* 2008; **80**: 878–85.
20 Deininger SO, Ebert MP, Futterer A, Gerhard M, Rocken C. MALDI imaging combined with hierarchical clustering as a new tool for the interpretation of complex human cancers. *J Proteome Res* 2008; **7**: 5230–6.
21 Willems SM, van Remoortere A, van Zeijl R, Deelder AM, McDonnell LA, Hogendoorn PC. Imaging mass spectrometry of myxoid sarcomas identifies proteins and lipids specific to tumour type and grade, and reveals biochemical intratumour heterogeneity. *J Pathol* 2010; **222**: 400–9.
22 Kahyo T, Iwaizumi M, Shinmura K *et al.* A novel tumor-derived SGOL1 variant causes abnormal mitosis and unstable chromatid cohesion. *Oncogene* 2011; **30**: 4453–63.
23 Sugimura H, Mori H, Nagura K *et al.* Fluorescence in situ hybridization analysis with a tissue microarray: 'FISH and chips' analysis of pathology archives. *Pathol Int* 2010; **60**: 543–50.
24 Okudela K, Yazawa T, Ishii J *et al.* Down-regulation of FXYD3 expression in human lung cancers: its mechanism and potential role in carcinogenesis. *Am J Pathol* 2009; **175**: 2646–56.
25 Costa WH, Rocha RM, Cunha IW, Guimaraes GC, Zequi Sde C. Immunohistochemical expression of CD44s in renal cell carcinoma lacks independent prognostic significance. *Int Braz J Urol* 2012; **38**: 456–65.
26 Natsume H, Shinmura K, Tao H *et al.* The CRKL gene encoding an adaptor protein is amplified, overexpressed, and a possible therapeutic target in gastric cancer. *J Transl Med* 2012; **10**: 97.
27 Garrett TJ, Yost RA. Analysis of intact tissue by intermediate-pressure MALDI on a linear ion trap mass spectrometer. *Anal Chem* 2006; **78**: 2465–9.
28 Hayasaka T, Goto-Inoue N, Sugiura Y *et al.* Matrix-assisted laser desorption /ionization quadrupole ion trap time-of-flight (MALDI-QIT-TOF)-based imaging mass spectrometry reveals a layered distribution of phospholipid molecular species in the mouse retina. *Rapid Commun Mass Spectrom* 2008; **22**: 3415–26.
29 Al-Saad KA, Siems WF, Hill HH, Zabrouskov V, Knowles NR. Structural analysis of phosphatidylcholines by post-source decay matrix-assisted laser desorption/ionization time-of-flight mass spectrometry. *J Am Soc Mass Spectrom* 2003; **14**: 373–82.
30 Chen X, Hyatt BA, Mucenski ML, Mason RJ, Shannon JM. Identification and characterization of a lysophosphatidylcholine acyltransferase in alveolar type II cells. *Proc Natl Acad Sci U S A* 2006; **103**: 11724–9.
31 Shindou H, Hishikawa D, Nakanishi H *et al.* A single enzyme catalyzes both platelet-activating factor production and membrane biogenesis of inflammatory cells. Cloning and characterization of acetyl-CoA:LYSO-PAF acetyltransferase. *J Biol Chem* 2007; **282**: 6532–9.
32 Zhao Y, Chen YQ, Bonacci TM *et al.* Identification and characterization of a major liver lysophosphatidylcholine acyltransferase. *J Biol Chem* 2008; **283**: 8258–65.
33 Hishikawa D, Shindou H, Kobayashi S, Nakanishi H, Taguchi R, Shimizu T. Discovery of a lysophospholipid acyltransferase family essential for membrane asymmetry and diversity. *Proc Natl Acad Sci U S A* 2008; **105**: 2830–5.
34 Gijon MA, Riekhof WR, Zarini S, Murphy RC, Voelker DR. Lysophospholipid acyltransferases and arachidonate recycling in human neutrophils. *J Biol Chem* 2008; **283**: 30235–45.
35 Hayasaka T, Goto-Inoue N, Ushijima M *et al.* Development of imaging mass spectrometry (IMS) dataset extractor software. IMS convolution. *Anal Bioanal Chem* 2011; **401**: 183–93.
36 Setou M. *Imaging Mass Spectrometry: Protocols for Mass Microscopy*, 1st edn. Tokyo, Japan: Springer, 2010.
37 Setou M, Kurabe N. Mass microscopy: high-resolution imaging mass spectrometry. *J Electron Microsc (Tokyo)* 2011; **60**: 47–56.
38 Jain S, Zhang X, Khandelwal PJ, Saunders AJ, Cummings BS, Oelkers P. Characterization of human lysophospholipid acyltransferase 3. *J Lipid Res* 2009; **50**: 1563–70.

Supporting Information

Additional Supporting Information may be found in the online version of this article:

Fig. S1. Involvement of LPCAT4 in the synthesis of PC(16:0/16:1) in DLD1 *in vitro*.

Fig. S2. Immunohistochemical analysis of the expression of LPCAT4 in adenomatous polyp.

Table S1. Clinicopathological profile of the cases on tissue microarray.

Table S2. Clinicopathological profile of polyps.

Table S3. Correlation of intensities generated using a mass microscope and immunohistochemical score.

Supplementary Methods. Including: LPCAT assay; immunohistochemistry; RNAi; and RT-PCR.

doi: 10.1111/cas.12221

Pathology International

Pathology International 2013; **63**: 195–200 doi:10.1111/pin.12050

Rapid Communication

Visualization of phosphatidylcholine (16:0/16:0) in type II alveolar epithelial cells in the human lung using imaging mass spectrometry

Nobuya Kurabe,[1] Takahiro Hayasaka,[2] Hisaki Igarashi,[1] Hiroki Mori,[5] Keigo Sekihara,[3] Hong Tao,[1] Hidetaka Yamada,[1] Tomoaki Kahyo,[1] Ippei Onishi,[1] Hiroe Tsukui,[1] Akikazu Kawase,[3] Shun Matsuura,[1,4] Yusuke Inoue,[1,4] Kazuya Shinmura,[1] Kazuhito Funai,[3] Mitsutoshi Setou[2] and Haruhiko Sugimura[1]

Departments of [1]Tumor Pathology, [2]Cell Biology and Anatomy, [3]Surgery I and [4]Internal Medicine II, Hamamatsu University School of Medicine, and [5]Department of Pathology, Hamamatsu Medical Center, Hamamatsu, Shizuoka, Japan

Imaging mass spectrometry (MS) is an emerging technique that can detect numerous biomolecular distributions in a non-targeting manner. In the present study, we applied a mass imaging modality, mass microscopy, to human lung tissue and identified several molecules including surfactant constituents in a specific structure of the lung alveoli. Four peaks were identified using imaging MS, and the ion at *m/z* 772.5, in particular, was localized at some spots in the alveolar walls. Using an MS/MS analysis, the ion was identified as phosphatidylcholine (PC)(16:0/16:0), which is the main component of lung surfactant. In a larger magnification of the lung specimen, PC (16:0/16:0) was distributed in a mottled fashion in a section of the lung. Importantly, the distribution of PC (16:0/16:0) was identical to that of anti-SLC34A2 antibody immunoreactivity, which is known to be a specific marker of type II alveolar epithelial cells, in the same section. Our experience suggests that imaging MS has excellent potential in human pathology research.

Key words: imaging mass spectrometry, mass microscope, phosphatidylcholine, pulmonary surfactant, SLC34A2

Pulmonary alveoli are mainly composed of two cell types: alveolar type I epithelial cells cover 95% of the surface of alveoli, while alveolar type II epithelial cells secrete pulmonary surfactant. Pulmonary surfactant is a lipoprotein, consisting of disaturated phosphatidylcholine (PC) and various surfactant proteins (SP-A, SP-B, SP-C and SP-D). The main role of lung surfactant is to reduce the tension of alveoli. The impairment of lung surfactant production causes severe respiratory failure in both children and adults with diseases such as respiratory distress syndrome.[1–3] As for surfactant protein, for example, the deletion of the SP-A gene is associated with the prognosis of patients with non-small cell lung cancer.[4] While studies of lipids in lung surfactant using pulmonary broncho-alveolar lavage fluid (BALF) or lung homogenate have been reported,[5,6] imaging studies are scarce; thus, the reality of pulmonary alveoli surfactant *in situ* remains unclear. Direct imaging mass spectrometry (MS) is a newly developed technique. The equipment used for imaging MS consists of a microscopic and mass spectrometric apparatus. Through two-dimensional scanning with a laser on the sample section, this technique enables us to visualize the localization of molecules under atmospheric conditions.[7] For the last decade, this technique has been applied to imaging and discovery tools, such as cancer-specific protein markers and tissue specific biomolecules.[8,9] Morita *et al.* demonstrated that histone H4 was highly expressed in poorly differentiated gastric carcinoma by scanning the tissue microarray (TMA) of formalin-fixed paraffin-embedded (FFPE) specimens by imaging MS.[8] Shimma *et al.* reported that imaging MS enabled the visualization and identification of phospholipis, glycolipid and tryptic-digested proteins in the mouse cerebellum specimens.[10] On the other hand, no tools have been available, until recently, for the detection or survey of lipid molecules in tissues. Actually, the generation of antibodies against lipids remains difficult even today, and genetic approaches are often not applicable to the study of lipids. Consequently, visualizing lipids has long been a great challenge for researchers. Recently, lipid imaging has gained popularity as a research tool for investigating lipids in various

Correspondence: Haruhiko Sugimura, MD, PhD, Department of Tumor Pathology, Hamamatsu University School of Medicine, 1-20-1 Handayama, Higashi Ward, Hamamatsu, Shizuoka 431-3192, Japan. Email: hsugimur@hama-med.ac.jp

The authors have no conflicts of interest to declare.

Received 5 December 2012. Accepted for publication 3 April 2013.

fields, since many scientists have noticed that the currently available imaging MS is especially powerful and feasible for detecting a wide range of biomolecules, including lipids.

To clarify the precise localization of surfactant lipid in normal alveoli, we used imaging MS to profile the lipid distribution of pulmonary surfactant. This study successfully identified, for the first time, the distribution of lipids in alveoli using imaging MS.

MATERIALS AND METHODS

Sample preparation

Three lung and one bronchial samples were retrieved from the archives of the Hamamatsu University Hospital. Non-diseased portions of the lung obtained from lung surgical specimens and autopsy specimens were snap-frozen in liquid nitrogen and stored at −80°C until required. Before sectioning, the frozen tissue blocks were left for 30 min at −20°C. The tissue sections were then cut to a thickness of 8 μm at −20°C using a cryostat (CM1950; Leica, Microsystems, Wetzlar, Germany). The tissue sections were stained with hematoxylin and eosin (HE) to identify the pulmonary alveoli. The adjacent sections were transferred onto indium-tin-oxide (ITO)-coated slide glasses (Bruker Daltonics, Billerica, MA, USA) and thawed. The tissue sections were then slowly brought to room temperature and uniformly coated with 2,5-dihydroxybenzoic acid (DHB; Bruker Daltonics) in 70% methanol and 10 mM potassium acetate using a 0.2-mm nozzle airbrush (Procon Boy FWA Platinum; Mr Hobby, Tokyo, Japan).[11]

Imaging MS analysis

All imaging MS analyses were performed using atmospheric pressure (AP)-matrix assisted laser desorption ionization (MALDI) with a quadrupole ion trap (QIT)-time of flight (TOF) analyzer instrument: a mass microscope equipped with a diode-pumped 355-nm Nd:YAG laser (Shimadzu, Kyoto, Japan).[12] All the mass spectra were acquired using mass microscope System software (Shimadzu). The sample was irradiated with a focused laser beam in synchrony with the stage scanning. The mass spectrum was then acquired for each spot on the tissue section. In this manner, ion images showing the distribution of biomolecules within the samples were obtained. The measurements were performed in reflectron mode within a mass range of *m/z* 700–850 using a scan pitch of 7.5 μm (for ×20 magnification) or 20 μm (for ×2.5 magnification) pixel size. The laser shot number and frequency were 200 per pixel and 1000 Hz, respectively. Lipid peak assignments were made by comparing the peak's mass measurement with the LIPID MAPS database (http://lipidmaps.org) and were confirmed using an MS/MS analysis (QSTAR Elite; Applied Biosystems, Foster City, CA, USA). Image reconstruction was performed using the software BioMap (freeware: http://www.maldi-msi.org).[10]

Immunohistochemistry

Tissue preparation and immunohistochemical analyses of the lung specimens were performed as previously described.[13] Following the measurements, the matrix was removed with 70% ethanol and the sections were stained using immunohistochemistry. After matrix removal, the sections were immersed in a 0.3% hydrogen peroxide solution to inhibit endogenous peroxidase activity. For antigen retrieval, the slides were heated at 96°C for 30 min in TE buffer (pH 9.0), followed by incubation at room temperature for 30 min. Affinity-isolated rabbit anti-SLC34A2 antibody (1:500; Sigma, St. Louis, MO, USA) was used. Next, the sections were treated with a peroxidase-conjugated secondary antibody (Histofine Simple Stain MAX PO; Nichirei, Japan) followed by incubation at room temperature for 30 min. For color reactions, the sections were incubated with diaminobenzidine (DAB) Substrate-Chromogen Solution (DAKO Cytomation; Carpinteria, CA, USA) and the sections were counterstained with 0.1% hematoxylin. Following immunohistochemistry, the sections were photographed using Keyence BZ-9000 (Keyence, Tokyo, Japan). The stained sections were co-registered with the imaging MS results and were evaluated histologically by performing a conventional histopathological analysis.

Ethical considerations

The study protocol was approved by the Institutional Review Board of Hamamatsu University School of Medicine (approval 23–91).

RESULTS

To profile the lipid contents in the lung specimen directly, we performed imaging MS. The region of interest (ROI) in the lung specimens was determined based on the ordinary morphology revealed by HE staining (Fig. 1a). Figure 1(b) shows a representative mass spectrum for a lung specimen with four intense peaks (*m/z* 716.0, 737.0, 772.5 and 817.0). The *m/z* range from 700 to 850 was shown to be that of phosphatidylcholine,[14] which is a component of lung surfactant. Of the four peaks shown in Fig. 1(b), the most intense peak was the ion at *m/z* 772.5. To visualize the distribution of ion peaks,

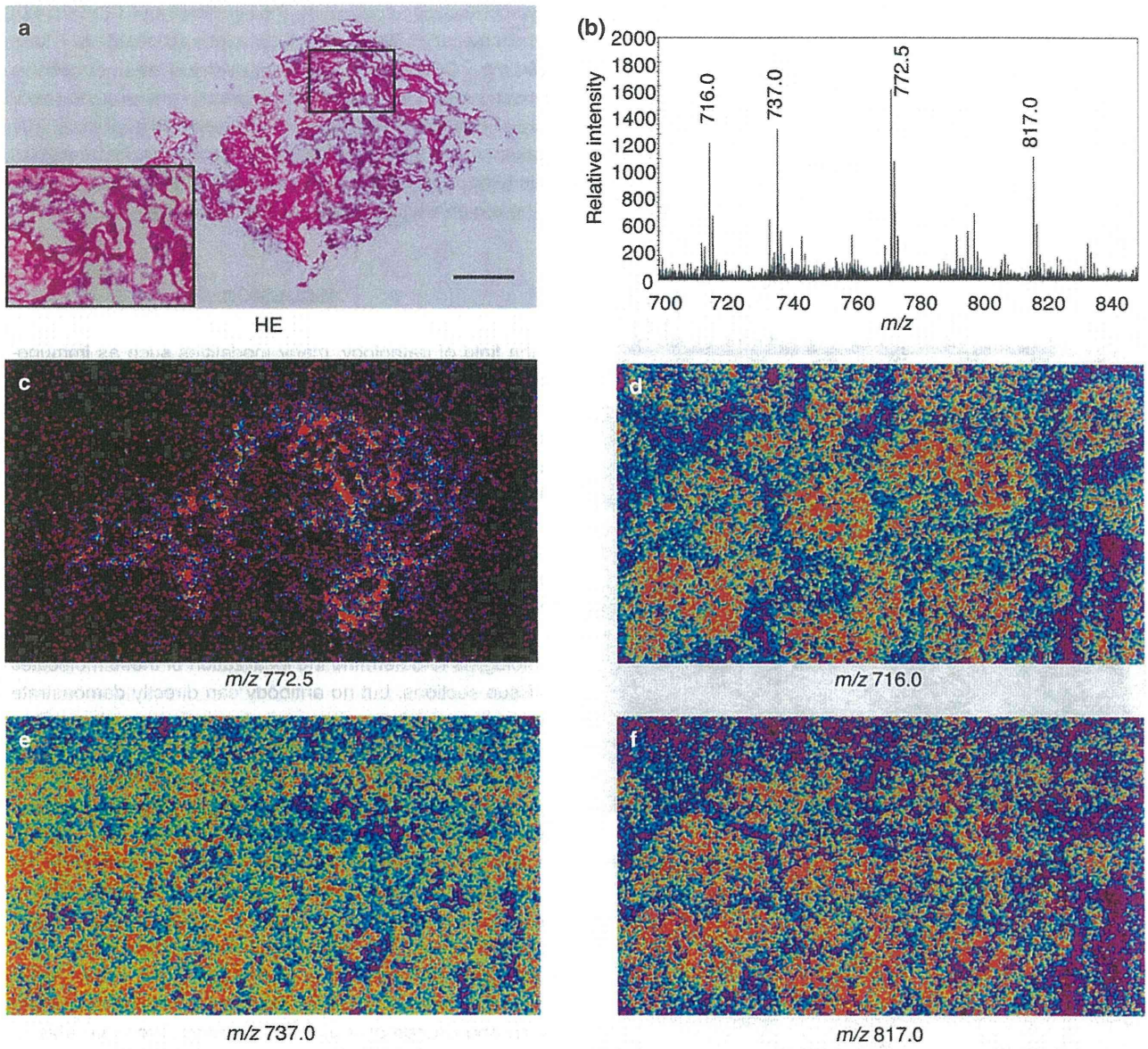

Figure 1 Imaging MS (mass spectrometry) analysis of a lung specimen. (**a**) HE (hematoxylin and eosin) staining of the lung specimen. Scale bar, 500 μm. inset, magnified view of the lung specimen. (**b**) Representative spectra obtained from the lung specimen. The ion at *m/z* 772.5 (**c**), 716.0 (**d**), 737.0 (**e**), and 817.0 (**f**) were imaged using BioMap.

we imported the spectrum data into the imaging software BioMap. Figure 1(c) shows that the peak at *m/z* 772.5 was specifically localized within the lung specimen, while the remaining three peaks were uniformly distributed throughout the entire section (Fig. 1d–f). To identify the ion at *m/z* 772.5, we performed an MS/MS analysis. Figure 2(a) show the MS/MS spectrum obtained from normal lung specimens. LIPID MAPS was used as a reference. The ion at *m/z* 772.5 was assigned as [PC(16:0/16:0) + K^+] because neutral losses of 59 Da and 183 Da were observed, which is indicative of PC. The peak at *m/z* 163 corresponded to cyclophosphate (124 Da) and a potassium ion (39 Da). As shown in Fig. 2(b), PC(16:0/16:0) exhibited a spotty pattern on the alveolar wall when examined at a higher magnification. To specify the PC(16:0/16:0) localization more precisely, we performed an immunohistochemical analysis using an anti-SLC34A2 (solute carrier family 34 (sodium phosphate), member 2) antibody (Fig. 2b). SLC34A2 is specifically expressed in type II alveolar epithelial cells and is formally referred to as sodium-dependent phosphate transporter type IIb (NPT2b) in mice and NaPi-3b in human.[15–18] The PC(16:0/16:0) signal was colocalized with the SLC34A2 antibody

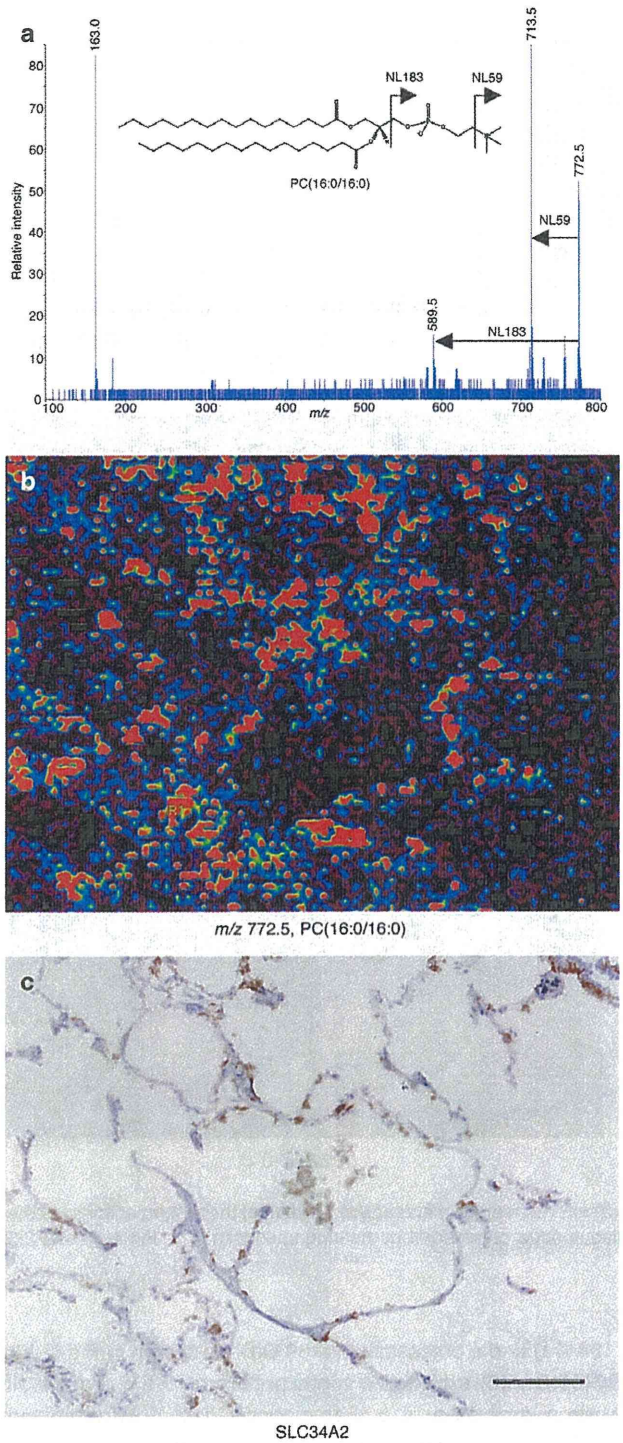

Figure 2 Ion assignment of *m/z* 772.5 and immunohistochemical analysis of a lung specimen. (**a**) An MS/MS analysis was performed to identify the ion at *m/z* 772.5. PC (phosphatidylcholine) (16:0/16:0) signals (**b**) were colocalized with the SLC34A2 antibody immunoreactivity (**c**). Scale bar, 100 μm.

immunoreactivity, suggesting the synthesis of PC(16:0/16:0) in the lamellar bodies of type II alveolar epithelial cells. Moreover, the PC(16:0/16:0) (Fig. 3a,d) signal was not observed in mass spectrum of bronchial specimen, revealing the specificity of PC(16:0/16:0) signal in alveolar epithelial cells. The peak at *m/z* 782.5, was localized at the bronchial epithelial cells (Fig. 3f) and the peaks at *m/z* 737.5 and 775.5, existed in the region without bronchial specimen (Fig. 3c,e).

DISCUSSION

In the field of pathology, many modalities such as immunohistochemistry using several modifications,[3] fluorescence *in situ* hybridization,[19,20] chromogenic *in situ* hybridizaition,[21] microRNA analysis,[22] and, finally, the comprehensive application of state-of-the-art genomic methods[23] are presently being used. Some of these technologies are already used in daily practice, while the future applications of others are being considered. The above-mentioned technologies, however, are still not completely satisfactory for the present needs of pathologists for reasons other than their cost alone. For example, antibodies against known molecules enable pathologists to determine the localization of these molecules in tissue sections, but no antibody can directly demonstrate the localization of an unknown molecule in a specimen. Furthermore, almost no antibodies are available for the detection of lipid molecules, which are important constituents of the human body. Thus, the development of techniques to detect the distributions of unknown molecules accurately is needed. MS and imaging MS have emerged as a useful option for the diagnosis and identification of unknown biomolecules. We previously reported the feasibility of imaging MS in various biological fields.[24–26] In the present study, we focused on the distribution of PC in pulmonary surfactant. PC is composed of many combinations of lipids and can be defined based on the length and degree of acyl chain satiation. We were able to detect the lipid species of PC successfully (Fig. 1). To date, other studies of BALF have provided limited information about the localization of lung surfactant lipid, however, the actual localization of lung surfactant lipid has never been observed. The present study demonstrated that the distribution of lipid surfactant PC(16:0/16:0) corresponded exactly with the distribution of type II alveolar epithelial cells, and we were able to demonstrate the luminal distribution of pulmonary surfactant (Figs 2,3).

In conclusion, to the best of our knowledge, this report is the first to present actual images of the distribution of pulmonary surfactant in alveoli. Our findings should pave the way to further applications of imaging MS in the investigation of lung pathophysiology related to lung surfactant and the function of surfactant in processes such as pulmonary proteinosis, pulmonary microlithiasis, acute respiratory distress syndrome in

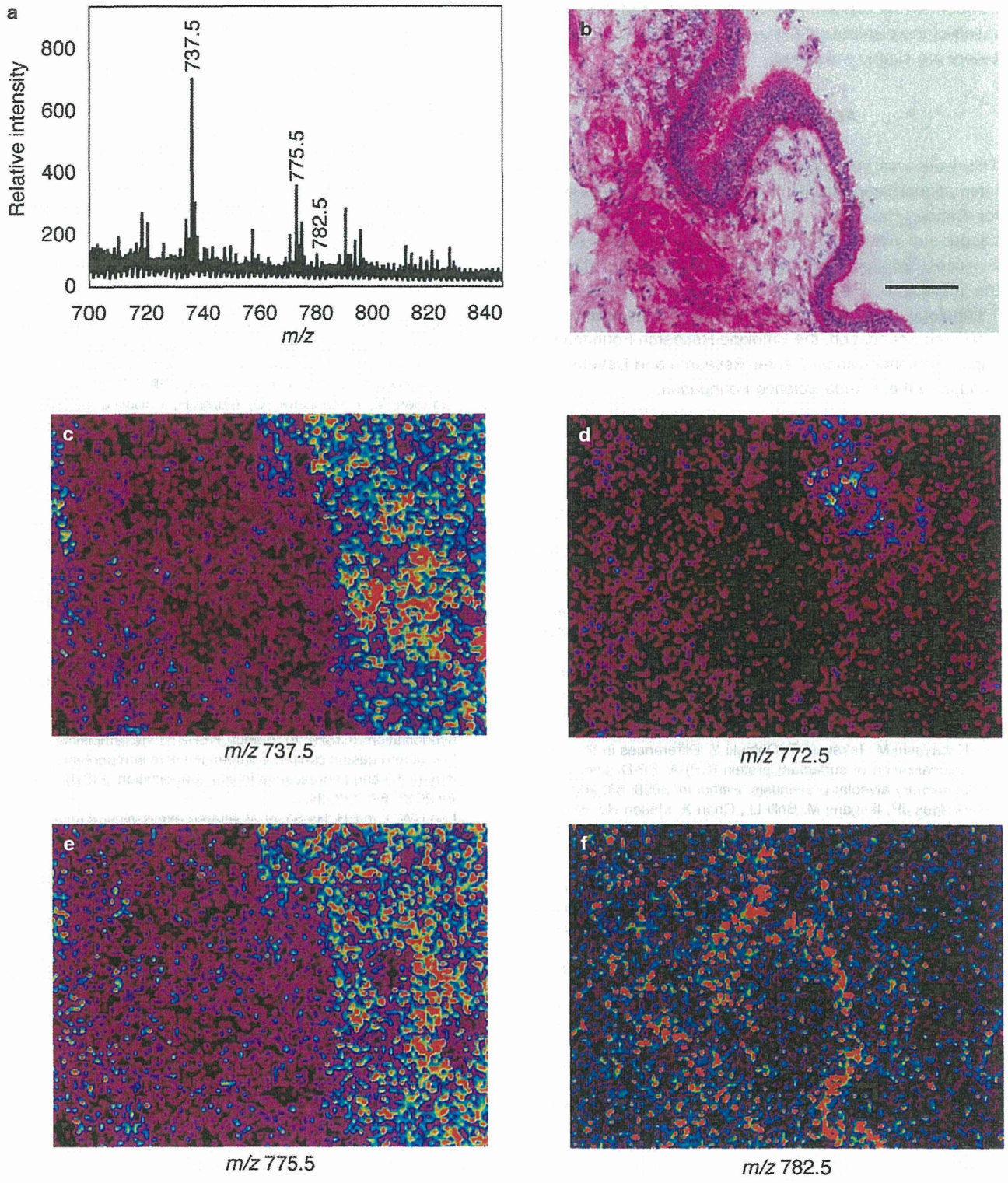

Figure 3 Imaging MS analysis of a bronchial specimen. (**a**) Representative spectra obtained from the bronchial specimen. (**b**) HE (hematoxylin and eosin) staining of the bronchial region. Scale bar, 100 μm. The ion at *m/z* 737.5 (**c**), 772.5 (**d**), 775.5 (**e**), and 782.5 (**f**) were imaged using BioMap.

newborns, and cancer. Further MS analyses of the deterioration of the distribution of surfactant in these diseases and others are clearly warranted.

ACKNOWLEDGMENTS

This work was supported by Grants-in-Aids (Research on International Cooperation in Medical Science, Grants-in-Aids for Cancer Research, 21-1) from the Ministry of Health, Labour and Welfare, the Japan Society for the Promotion of Science (22590356, 22790378, 23116510 and 20670004), the Ministry of Education, Culture, Sports, Science and Technology (221S0001), the Princess Takamatsu Cancer Research Foundation, the Smoking Research Foundation of Japan, National Cancer Center Research and Development Fund, and the Takeda Science Foundation.

REFERENCES

1 Farrell PM, Avery ME. Hyaline membrane disease. *Am Rev Respir Dis* 1975; **111**: 657–88.
2 Petty TL, Silvers GW, Paul GW, Stanford RE. Abnormalities in lung elastic properties and surfactant function in adult respiratory distress syndrome. *Chest* 1979; **75**: 571–4.
3 Pison U, Seeger W, Buchhorn R *et al.* Surfactant abnormalities in patients with respiratory failure after multiple trauma. *Am Rev Respir Dis* 1989; **140**: 1033–9.
4 Jiang F, Caraway NP, Nebiyou Bekele B *et al.* Surfactant protein A gene deletion and prognostics for patients with stage I non-small cell lung cancer. *Clin Cancer Res* 2005; **11**: 5417–24.
5 Kobayashi M, Takeuchi T, Ohtsuki Y. Differences in the immunolocalization of surfactant protein (SP)-A: SP-D, and KL-6 in pulmonary alveolar proteinosis. *Pathol Int* 2008; **58**: 203–7.
6 Bridges JP, Ikegami M, Brilli LL, Chen X, Mason RJ, Shannon JM. LPCAT1 regulates surfactant phospholipid synthesis and is required for transitioning to air breathing in mice. *J Clin Invest* 2010; **120**: 1736–48.
7 Kakimoto Y, Tsuruyama T, Yamamoto T *et al.* Novel in situ pretreatment method for significantly enhancing the signal in MALDI-TOF MS of formalin-fixed paraffin-embedded tissue sections. *PLoS One* 2012; **7**: e41607.
8 Cazares LH, Troyer D, Mendrinos S *et al.* Imaging mass spectrometry of a specific fragment of mitogen-activated protein kinase/extracellular signal-regulated kinase kinase kinase 2 discriminates cancer from uninvolved prostate tissue. *Clin Cancer Res* 2009; **15**: 5541–51.
9 Morita Y, Ikegami K, Goto-Inoue N *et al.* Imaging mass spectrometry of gastric carcinoma in formalin-fixed paraffin-embedded tissue microarray. *Cancer Sci* 2010; **101**: 267–73.
10 Shimma S, Sugiura Y, Hayasaka T, Zaima N, Matsumoto M, Setou M. Mass imaging and identification of biomolecules with MALDI-QIT-TOF-based system. *Anal Chem* 2008; **80**: 878–85.
11 Sugiura Y, Setou M. Selective imaging of positively charged polar and nonpolar lipids by optimizing matrix solution composition. *Rapid Commun Mass Spectrom* 2009; **23**: 3269–78.
12 Harada T, Yuba-Kubo A, Sugiura Y *et al.* Visualization of volatile substances in different organelles with an atmospheric-pressure mass microscope. *Anal Chem* 2009; **81**: 9153–7.
13 Igarashi H, Sugimura H, Maruyama K *et al.* Alteration of immunoreactivity by hydrated autoclaving, microwave treatment, and simple heating of paraffin-embedded tissue sections. *APMIS* 1994; **102**: 295–307.
14 Garrett TJ, Yost RA. Analysis of intact tissue by intermediate-pressure MALDI on a linear ion trap mass spectrometer. *Anal Chem* 2006; **78**: 2465–9.
15 Feild JA, Zhang L, Brun KA, Brooks DP, Edwards RM. Cloning and functional characterization of a sodium-dependent phosphate transporter expressed in human lung and small intestine. *Biochem Biophys Res Commun* 1999; **258**: 578–82.
16 Traebert M, Hattenhauer O, Murer H, Kaissling B, Biber J. Expression of type II Na-P(i) cotransporter in alveolar type II cells. *Am J Physiol* 1999; **277**: L868–73.
17 Hashimoto M, Wang DY, Kamo T *et al.* Isolation and localization of type IIb Na/Pi cotransporter in the developing rat lung. *Am J Pathol* 2000; **157**: 21–7.
18 Huqun, Izumi S, Miyazawa H *et al.* Mutations in the SLC34A2 gene are associated with pulmonary alveolar microlithiasis. *Am J Respir Crit Care Med* 2007; **175**: 263–8.
19 Sugimura H, Mori H, Nagura K *et al.* Fluorescence in situ hybridization analysis with a tissue microarray: 'FISH and chips' analysis of pathology archives. *Pathol Int* 2010; **60**: 543–50.
20 Sugimura H. Detection of chromosome changes in pathology archives: An application of microwave-assisted fluorescence in situ hybridization to human carcinogenesis studies. *Carcinogenesis* 2008; **29**: 681–7.
21 Kiyose S, Igarashi H, Nagura K *et al.* Chromogenic in situ hybridization (CISH) to detect HER2 gene amplification in breast and gastric cancer: Comparison with immunohistochemistry (IHC) and fluorescence in situ hybridization (FISH). *Pathol Int* 2012; **62**: 728–34.
22 Lee HW, Lee EH, Ha SY *et al.* Altered expression of microRNA miR-21, miR-155, and let-7a and their roles in pulmonary neuroendocrine tumors. *Pathol Int* 2012; **62**: 583–91.
23 Shibata T. Cancer genomics and pathology: All Together Now. *Pathol Int* 2012; **62**: 647–59.
24 Hayasaka T, Goto-Inoue N, Ushijima M *et al.* Development of imaging mass spectrometry (IMS) dataset extractor software, IMS convolution. *Anal Bioanal Chem* 2011; **401**: 183–93.
25 Setou M. *Imaging Mass Spectrometry: Protocols for Mass Microscopy*, 1st edn. New York: Springer, 2010.
26 Setou M, Kurabe N. Mass microscopy: High-resolution imaging mass spectrometry. *J Electron Microsc (Tokyo)* 2011; **60**: 47–56.

Genes to Cells

Establishment and characterization of a mutagenized cell line exhibiting the 'cell-in-cell' phenotype at a high frequency

Tomoaki Kahyo* and Haruhiko Sugimura

Department of Tumor Pathology, Hamamatsu University School of Medicine, 1-20-1 Handayama, Higashi-ku, Hamamatsu 431-3192, Japan

Cell-in-cell structures represent live cell events in which one cell internalizes another. Because formation of cell-in-cell structures is a rare event in most cell types and the event is associated with cell death, there has been limited clarification of this phenomenon, and its physiological role and molecular mechanism are yet to be precisely elucidated. In this study, we established a mutagenized cell line that exhibited cell-in-cell structures at a more than 10-fold higher frequency as compared to the parent cells. Interestingly, both engulfment and invasion were increased in the mutagenized cell line as compared with that in the parent cell line in the suspension culture condition. This finding indicates that this mutagenized cell line showed an interchangeable status in terms of its ability to form cell-in-cell structures, and the system described here could be useful for elucidation of the mechanisms regulating the formation of cell-in-cell structures, including engulfment and invasion, in a given cellular environment. Further studies using this cell line are warranted to understand the mechanism of formation and biological significance of the cell-in-cell formation.

Introduction

Cell-in-cell structures, with nested doll-like features, were referred to as 'bird's eye' more than a century ago (Bauchwitz 1981) and have been observed to involve various cell types (Overholtzer & Brugge 2008), including neutrophils in megakaryocytes (Lee 1989; Schmitt *et al.* 2000; Woulfe *et al.* 2008) and thymocytes in thymic nurse cells (Wekerle & Ketelsen 1980; Ritter *et al.* 1981; Martinez *et al.* 2007). Cell-in-cell interactions between these cells are often referred to as emperipolesis, which is a term used to describe the long-term movements of internalized cells (Humble *et al.* 1956) and has often been observed in Rosai–Dorfman disease, a rare, but well-defined histiocytic proliferative disorder (Iyer *et al.* 2009). As described by Humble *et al.*, in emperipolesis, the internalized cells often seem to be wandering around inside the host cells; therefore, emperipolesis is regarded as an event in which the targeted cells are alive and not dead, in contrast to phagocytosis, in which the engulfed cells are usually dead and pathogenic (Takeda & Akira 2001; Krysko & Vandenabeele 2010); however, the term 'emperipolesis' has sometimes been used to represent phagocytosis.

In addition to emperipolesis, the terms 'cell cannibalism' and 'entosis' have also been used to describe cell-in-cell structures. Cell cannibalism has been recognized mostly as an active engulfment event of host cancer cells (Brouwer *et al.* 1984). In contrast, entosis seems to be an event where a cell invades another cell more actively (Overholtzer *et al.* 2007). Cell-in-cell structures have also been observed in various tumors, including breast carcinoma, lung small-cell carcinoma and melanoma (Overholtzer & Brugge 2008), and have been suggested to be involved in the aggressiveness of the malignancy, although the pathological roles of cell-in-cell events in tumor biology remain unclear (Sharma & Dey 2011).

In cell-in-cell events, the host cells can internalize multiple cells (Steinhaus 1981) and also another host cell with an internalized cell (Overholtzer *et al.* 2007). Furthermore, an internalized cell can divide into two daughter cells even inside the host cell and also come out of the host cell (Overholtzer *et al.*

Communicated by: Yusaku Nakabeppu
**Correspondence:* kahyo@hama-med.ac.jp

DOI: 10.1111/gtc.12092